

Journal of Mechanics of Materials and Structures

**THERMAL STRESS AROUND AN ARBITRARY SHAPED NANO HOLE
WITH SURFACE ELASTICITY IN A THERMOELECTRIC MATERIAL**

Kun Song, Hao-Peng Song, Peter Schiavone and Cun-Fa Gao

Volume 14, No. 4

July 2019



THERMAL STRESS AROUND AN ARBITRARILY SHAPED NANO HOLE WITH SURFACE ELASTICITY IN A THERMOELECTRIC MATERIAL

KUN SONG, HAO-PENG SONG, PETER SCHIAVONE AND CUN-FA GAO

In response to the significance of the role of surface mechanics in continuum models of deformation at the nanoscale, we consider the thermal stress distribution in the vicinity of an arbitrarily shaped nanohole in a thermoelectric material by incorporating the contribution of surface elasticity. Accordingly, we develop specific solutions describing the corresponding electric, temperature and elastic fields in the material. Our results indicate that the contribution of surface elasticity is to generate considerable normal and shear stress and to significantly influence hoop stress on the boundary of the nanohole. By controlling the electric current applied to the material, the normal and shear stresses induced by surface elasticity can be enhanced or decreased for various shaped nanoholes. It is also worth noting that the incorporation of surface elasticity allows for the ability to suppress the maximum value of the von Mises stress on the boundary of an arbitrarily shaped nanohole, particularly in the case of a triangular-shaped hole in which case the maximum von Mises stress can be suppressed by up to 35% thereby dramatically improving the reliability of the corresponding thermoelectric device. Our investigations provide an important theoretical basis for the design and manufacture of thermoelectric materials.

1. Introduction

Thermoelectric materials have the distinct capability of direct conversion between thermal and electrical energy. This particular property makes them attractive for use in a variety of fields of application including waste heat recovery [Yu et al. 2015], solid-state refrigeration [He and Tritt 2017] and solar energy harvesting [Özdemir et al. 2015]. Furthermore, thermoelectric systems are environmentally friendly in that they emit no gases, contain no pollutants, have no moving parts and operate quietly. One of the major drawbacks in the use of thermoelectric materials and the main factor in preventing thermoelectric devices from replacing traditional heat engines, however, is a low energy conversion efficiency.

The thermoelectric figure of merit ZT was introduced to characterize the conversion efficiency of thermoelectric materials and much effort has been devoted recently towards its improvement. The most effective and widely used method to improve the ZT value of a thermoelectric material involves the introduction of nanosized holes or inclusions into the thermoelectric medium. This method has achieved remarkable results in many mainstream thermoelectric materials [Yang et al. 2015; Xu et al. 2017; Kim et al. 2006] but suffers from the fact that the operation of inserting an inhomogeneity (here taken to represent a hole or inclusion) into thermoelectric materials generates an uneven temperature distribution which leads to considerable thermal stress in the vicinity of the inhomogeneity [Kim et al. 2016].

Keywords: thermoelectric material, thermal stress, arbitrarily shaped hole, surface elasticity.

The theoretical modelling of the behavior of thermoelectric materials presents formidable challenges over the modeling of simple electric conduction or heat transfer processes mainly due to the coupled transport of heat and electricity which results in nonlinear governing equations. Using complex variable methods, Song et al. [2015] have succeeded in deriving the general solution of the two-dimensional problem of a thermoelectric material containing a crack and discussed the field intensity factors at the crack tip. Soon after, Wang and Wang [2017] used the same methods to construct a theoretical model for the thermal stress distribution around an inclined elliptic hole in a thermoelectric material. Subsequently, the model of a thin infinite plate containing a circular hole with a straight crack was analyzed and the stress intensity factors near the crack tip obtained [Pang et al. 2018]. Furthermore, it has been demonstrated that the thermal stress around a functional defect can easily exceed the yield stresses of many thermoelectric materials [Song et al. 2019a]. These researches provide useful information regarding the mechanism controlling thermal stress around a macroscale hole or inhomogeneity in a thermoelectric material. The corresponding analysis focusing on a thermoelectric continuum at the nanoscale remains relatively absent from the literature.

At the nanoscale, it is well-known that surface effects significantly influence the corresponding stress distributions around an inhomogeneity as a result of the large surface-to-volume ratio of a representative material element [Attia 2017]. Acknowledging the increasingly important role of the use of nanosized inhomogeneities in improving the conversion efficiency of thermoelectric materials, it is important to study the reliability of thermoelectric continuum models at the nanoscale. To this end, in this paper we focus our attention on the thermal stress distribution in the vicinity of an arbitrarily shaped nanohole in a thermoelectric material. General solutions describing thermal-electric and thermoelastic fields are obtained via the use of complex variable methods. Our results indicate quite clearly that the incorporation of surface elasticity generates considerable normal and shear stresses on the boundary of various shaped nanoholes and that these stresses can be either increased or decreased by controlling the applied electric current depending on the shape of nanohole. Furthermore, we find that surface elasticity has also a remarkable effect on hoop stress around a nanohole and can dramatically suppress von Mises stress induced by heat flux. For example, the incorporation of surface elasticity can suppress the maximum von Mises stress around a particular triangular hole by about 35%. These results dramatically improve the reliability of the corresponding thermoelectric devices.

2. Governing equations

2.1. Electric and thermal fields. The temperature field $T(x, y)$ and electric potential $\phi(x, y)$ in a thermoelectric material represented by a Cartesian plane (described here by the generic point (x, y)) are coupled through the Seebeck coefficient S . According to the theory of Thermodynamics, the equations governing the electric current density \mathbf{J} , heat flux \mathbf{Q} and energy flux \mathbf{U} are given by [Callen 1960]

$$-\mathbf{J} = \sigma \nabla \phi + \sigma S \nabla T, \quad (1)$$

$$\mathbf{Q} = T S \mathbf{J} - \kappa \nabla T, \quad (2)$$

$$\mathbf{U} = \mathbf{Q} + \phi \mathbf{J}, \quad (3)$$

where σ and κ are the electric conductivity and thermal conductivity, respectively. In the case of a conserved system, both the electric current density and energy flux are divergence-free:

$$\nabla \cdot \mathbf{J} = 0, \quad (4)$$

$$\nabla \cdot (\mathbf{Q} + \phi \mathbf{J}) = 0. \quad (5)$$

We assume that the parameters of our system are temperature-independent, so that (4)–(5) can be rewritten with the aid of (1)–(2) as

$$\nabla^2(\phi + ST) = 0, \quad (6)$$

$$\nabla^2 \left[\frac{\sigma}{2} (\phi^2 + ST)^2 + \kappa T \right] = 0. \quad (7)$$

In the complex plane described by $z = x + iy$ ($i^2 = -1$), the temperature field and the electric potential in (6) and (7) can be expressed as [Song et al. 2018]

$$T = -\frac{\sigma}{\kappa} f(z) \overline{f(z)} + g(z) + \overline{g(z)} + M, \quad (8)$$

$$\phi = \frac{\sigma S}{\kappa} f(z) \overline{f(z)} + f(z) + \overline{f(z)} - S(g(z) + \overline{g(z)}) + N, \quad (9)$$

where $f(z)$ and $g(z)$ are complex analytic functions while M and N are real constants that denote uniform temperature and electric potential fields, respectively. Note that the overhead bar denotes the usual complex conjugate. Substituting (8)–(9) into (1)–(3), the components of electric current density, heat flux and energy flux can be expressed as

$$J_x - iJ_y = -2\sigma f'(z), \quad (10)$$

$$Q_x - iQ_y = 2\sigma f'(z) \left[\frac{\sigma S}{\kappa} f(z) \overline{f(z)} + f(z) + \overline{f(z)} - S(g(z) + \overline{g(z)}) + N \right] - 2\sigma f(z) f'(z) - 2\kappa g'(z), \quad (11)$$

$$U_x - iU_y = -2\sigma f(z) f'(z) - 2\kappa g'(z). \quad (12)$$

From (8)–(12), we see that the quantities corresponding to the thermal and electric fields are governed entirely by the complex functions $f(z)$ and $g(z)$. As such, the temperature distribution, electric potential, electric current, heat flow and energy flux in the thermoelectric material are known entirely if the two complex functions $f(z)$ and $g(z)$ are determined.

2.2. Stress and displacement fields. Thermal stress induced by unmatched thermal expansion in a thermoelectric material depends linearly on the thermal expansion coefficient α , leading to the governing equation coupling the stress function Φ and the temperature field T [Parkus 1968]:

$$\nabla^4 \Phi + E\alpha \nabla^2 T = 0, \quad (13)$$

where E is Young's modulus. The general solution of (13) is composed of a particular solution and the general solution of the corresponding homogeneous equation which is given as [Song et al. 2019c]

$$\Phi = \frac{1}{2} [\bar{z} \varphi(z) + z \overline{\varphi(z)} + \vartheta(z) + \overline{\vartheta(z)}] + \frac{E\alpha\sigma}{4\kappa} F(z) \overline{F(z)}, \quad (14)$$

where $\varphi(z)$ and $\vartheta(z)$ are complex analytic functions of z , and

$$F(z) = \int f(z) dz. \quad (15)$$

We introduce $\psi(z)$ to represent the derivative of $\vartheta(z)$. The stress and displacement components $\sigma_x, \sigma_y, \tau_{xy}$; u and v can then be derived from (14) as [Zhang and Wang 2016]

$$\sigma_x + \sigma_y = 4 \frac{\partial^2 \Phi}{\partial z \partial \bar{z}} = 2(\varphi'(z) + \overline{\varphi'(z)}) + \frac{E\alpha\sigma}{\kappa} f(z) \overline{f(z)}, \quad (16)$$

$$\sigma_y - \sigma_x + 2i\tau_{xy} = 4 \frac{\partial^2 \Phi}{\partial z^2} = 2(\bar{z}\varphi''(z) + \psi'(z)) + \frac{E\alpha\sigma}{\kappa} f'(z) \overline{f(z)}, \quad (17)$$

$$u + iv = \frac{1}{2G} [K\varphi(z) - z\overline{\varphi'(z)} - \overline{\psi(z)}] + 2\alpha \int g(z) dz - \frac{E\alpha\sigma}{4\kappa G} F(z) \overline{f(z)}, \quad (18)$$

where $K = (3 - \mu)/(1 + \mu)$ for the plane stress problem while G and μ are the shear modulus and Poisson's ratio, respectively. Note that E, μ and α are respectively replaced by $E/(1 - \mu^2), \mu/(1 - \mu)$ and $(1 + \mu)\alpha$ in the case of the plane strain problem.

2.3. Surface elasticity. The effects of surface elasticity are generally disregarded in the modelling of thermoelectric materials at the macroscale. However, it is well-known that the incorporation of surface elasticity into models of deformation significantly affects the stress distribution on the surface of a nanoinhomogeneity due to the large surface to volume ratio of a representative material element. According to the continuum theory of elastic material surfaces, the surface hoop stress σ_θ^s is a critical quantity in the description of surface elasticity and depends linearly on the hoop strain ε_θ^s , that is [Gurtin and Murdoch 1975]

$$\sigma_\theta^s = M^s \varepsilon_\theta^s, \quad (19)$$

where $M^s = 2\mu^s + \lambda^s$ is a surface material constant incorporating μ^s and λ^s which are referred to as surface Lamé constants. Noting (16)–(18), ε_θ^s can be expressed as [Dai et al. 2017]

$$\begin{aligned} \varepsilon_\theta^s = \frac{1 - \mu}{E} \left(\varphi'(z) + \overline{\varphi'(z)} + \frac{E\alpha\sigma}{2\kappa} f(z) \overline{f(z)} \right) + \frac{\operatorname{Re}[(\bar{z}\varphi''(z) + \psi'(z))e^{2i\theta}]}{2G} \\ + \frac{E\alpha\sigma}{4G\kappa} \operatorname{Re}[f'(z) \overline{f(z)} e^{2i\theta}] + 2\alpha \operatorname{Re}[g(z)], \end{aligned} \quad (20)$$

where the angle θ is measured from the x -axis, and “Re” denotes the real part of a complex function.

3. Solution for infinite thermoelectric plate containing an arbitrary shaped nanohole

We consider an infinite thermoelectric plate containing an arbitrarily shaped hole bounded by a simple curve L . The plate is subjected to remote electric current density J_x^∞, J_y^∞ and energy flux U_x^∞, U_y^∞ . Without loss of generality, the origin of the Cartesian coordinate system is placed at the centroid of the hole, as shown in Figure 1 (left). The infinite thermoelectric matrix surrounding the hole can be mapped into the external of a unit circle L' in the image w -plane ($w = \xi + i\eta$), as shown in Figure 1 (right), using

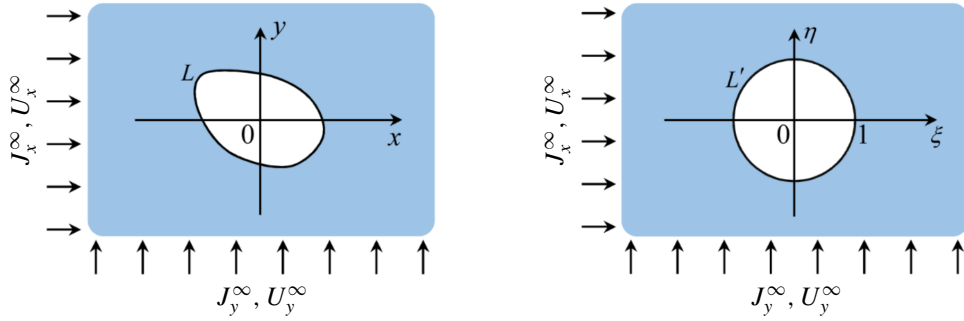


Figure 1. Left: infinite thermoelectric plate containing an arbitrarily shaped nanohole. Right: the image w -plane after conformal mapping.

the conformal mapping function $\omega(w)$ given by [Muskhelishvili 1975]

$$z = \omega(w) = R \left(w + \sum_{j=1}^n m_j w^{-j} \right), \quad (21)$$

where R is real number associated with the size of hole and the complex number m_j is determined by the shape of hole.

3.1. Boundary conditions. We assume that the boundary of the nanohole prevents the transport of both electrons and heat, thus the boundary conditions for the normal electric current density J_r and energy flux U_r can be written as [Song et al. 2019b]

$$\int_P^Q J_r ds = 0, \quad (22)$$

$$\int_P^Q U_r ds = 0, \quad (23)$$

where P and Q are arbitrary points on L .

As stated in Section 2.3, the presence of surface elasticity influences the stress field on the surface of a nanohole. Since there is no additional loading on the boundary L , the stress boundary conditions can be expressed as [Gurtin et al. 1998]

$$\sigma_r - i \tau_{r\theta} = k \sigma_\theta^s - i \frac{d\sigma_\theta^s}{ds}, \quad (24)$$

where σ_r and $\tau_{r\theta}$ are the normal and shear stresses on L , respectively, while k is the pointwise curvature along L .

3.2. Solutions for electric and thermal fields. The functions $f(z)$ and $g(z)$ can be deduced from (10) and (12) in terms of the remote current density and energy flux as

$$f(z) = -\frac{1}{2\sigma} (J_x^\infty - i J_y^\infty) z + f_0(z), \quad (25)$$

$$g(z) = -\frac{1}{8\sigma\kappa} (J_x^\infty - i J_y^\infty)^2 z^2 - \frac{1}{2\kappa} (U_x^\infty - i U_y^\infty) z + g_0(z), \quad (26)$$

where $f_0(z)$ and $g_0(z)$ are analytic functions in the matrix. Noting the conformal mapping function in (21) and adopting the notation that $f(z) = f[\omega(w)]$ and $g(z) = g[\omega(w)]$, equations (25) and (26) can be expanded into series form as

$$f(z) = A_1 w + \sum_{j=0}^n A_{-j} w^{-j}, \quad (27)$$

$$g(z) = B_2 w^2 + B_1 w + \sum_{j=0}^n B_{-j} w^{-j}, \quad (28)$$

where

$$A_1 = -\frac{R}{2\sigma}(J_x^\infty - iJ_y^\infty), \quad B_1 = -\frac{R}{2\kappa}(U_x^\infty - iU_y^\infty), \quad B_2 = -\frac{R^2}{8\sigma\kappa}(J_x^\infty - iJ_y^\infty)^2. \quad (29)$$

Substituting (27) and (28) into the boundary conditions in (22) and (23), $f(z)$ and $g(z)$ can be determined as

$$f(z) = A_1 w + \frac{\bar{A}_1}{w}, \quad (30)$$

$$g(z) = B_2 w^2 + B_1 w + \frac{\bar{B}_1}{w} + \frac{\bar{B}_2}{w^2}. \quad (31)$$

The temperature, electric potential, electric current density, heat flux and energy flux around an arbitrarily shaped nanohole in a thermoelectric material can then be totally determined by substituting (30) and (31) into (8)–(12) as

$$T = -\frac{\sigma}{\kappa} \left| A_1 w + \frac{\bar{A}_1}{w} \right|^2 + 2\operatorname{Re} \left[B_2 w^2 + B_1 w + \frac{\bar{B}_1}{w} + \frac{\bar{B}_2}{w^2} \right] + M, \quad (32)$$

$$\phi = \frac{\sigma S}{\kappa} \left| A_1 w + \frac{\bar{A}_1}{w} \right|^2 + 2\operatorname{Re} \left[A_1 w + \frac{\bar{A}_1}{w} - S \left(B_2 w^2 + B_1 w + \frac{\bar{B}_1}{w} + \frac{\bar{B}_2}{w^2} \right) \right] + N, \quad (33)$$

$$J_x - iJ_y = -\frac{2\sigma}{\omega'(w)} \left(A_1 - \frac{\bar{A}_1}{w^2} \right), \quad (34)$$

$$\begin{aligned} Q_x - iQ_y = & \frac{2\sigma\phi}{\omega'(w)} \left(A_1 - \frac{\bar{A}_1}{w^2} \right) - \frac{2\sigma}{\omega'(w)} \left(A_1 w + \frac{\bar{A}_1}{w} \right) \left(A_1 - \frac{\bar{A}_1}{w^2} \right) \\ & - \frac{2\kappa}{\omega'(w)} \left(2B_2 w + B_1 - \frac{\bar{B}_1}{w^2} - \frac{2\bar{B}_2}{w^3} \right), \end{aligned} \quad (35)$$

$$U_x - iU_y = \frac{2\sigma}{\omega'(w)} \left(A_1 w + \frac{\bar{A}_1}{w} \right) \left(\frac{\bar{A}_1}{w^2} - A_1 \right) - \frac{2\kappa}{\omega'(w)} \left(2B_2 w + B_1 - \frac{\bar{B}_1}{w^2} - \frac{2\bar{B}_2}{w^3} \right), \quad (36)$$

where $\omega'(w) = d\omega(w)/dw$.

3.3. Solution for stress distributions. Substituting (30) and (31) into (16)–(18), the thermal stress and displacement in the matrix can be expressed as

$$\sigma_x + \sigma_y = \frac{E\alpha\sigma}{\kappa} \left| A_1 w + \frac{\bar{A}_1}{w} \right|^2 + 2(\varphi'(z) + \overline{\varphi'(z)}), \quad (37)$$

$$\sigma_y - \sigma_x + 2i\tau_{xy} = \frac{E\alpha\sigma(A_1 w^2 - \bar{A}_1)}{\kappa w^2 \omega'(w)} \int \left[\left(\bar{A}_1 \bar{w} + \frac{A_1}{\bar{w}} \right) \overline{\omega'(w)} \right] d\bar{w} + 2(\bar{z}\varphi''(z) + \psi'(z)), \quad (38)$$

$$u + iv = 2\alpha \int \left[\left(B_2 w^2 + B_1 w + \frac{\bar{B}_1}{w} + \frac{\bar{B}_2}{w^2} \right) \omega'(w) \right] dw + \frac{1}{2G} (K\varphi(z) - z\overline{\varphi'(z)} - \overline{\psi(z)}) \\ - \frac{E\alpha\sigma}{4\kappa G} \left(\bar{A}_1 \bar{w} + \frac{A_1}{\bar{w}} \right) \int \left[\left(A_1 w + \frac{\bar{A}_1}{w} \right) \omega'(w) \right] dw, \quad (39)$$

while the hoop strain in (20) can be expressed as

$$\varepsilon_\theta^s = \frac{1-\mu}{E} \left(\varphi'(z) + \overline{\varphi'(z)} + \frac{E\alpha\sigma}{2\kappa} \left| A_1 w + \frac{\bar{A}_1}{w} \right|^2 \right) + \frac{\operatorname{Re}[(\bar{z}\varphi''(z) + \psi'(z))e^{2i\theta}]}{2G} \\ + \frac{E\alpha\sigma}{4G\kappa} \operatorname{Re} \left[\frac{(A_1 w^2 - \bar{A}_1)}{w^2 \omega'(w)} \int \left[\left(\bar{A}_1 \bar{w} + \frac{A_1}{\bar{w}} \right) \overline{\omega'(w)} \right] d\bar{w} e^{2i\theta} \right] \\ + 2\alpha \operatorname{Re} \left[B_2 w^2 + B_1 w + \frac{\bar{B}_1}{w} + \frac{\bar{B}_2}{w^2} \right]. \quad (40)$$

The integrations in (38)–(40) will generate multivalued terms which can be eliminated by introducing additional terms in $\varphi(z)$ and $\psi(z)$ as

$$\varphi(z) = \chi_1 \ln w + \sum_{j=1}^n C_{-j} w^{-j}, \quad (41)$$

$$\psi(z) = \chi_2 \ln w + \sum_{j=1}^n D_{-j} w^{-j}. \quad (42)$$

Here, we have disregarded C_0 and D_0 in (41) and (42) since they correspond to rigid displacement and thus do not influence the stresses. Noting (21), the coefficients of the multivalued terms are now identified as

$$\begin{cases} \chi_1 = \frac{4G\alpha R}{\kappa+1} (m_1 B_1 + 2m_2 B_2 - \bar{B}_1), \\ \chi_2 = \bar{\chi}_1 + \frac{E\alpha\sigma R}{2\kappa} (A_1 - m_1 \bar{A}_1) \left(A_1 w + \frac{\bar{A}_1}{w} \right). \end{cases} \quad (43)$$

Rewriting the boundary condition in (24), we have [Dai et al. 2016]

$$\varphi(z) + z\overline{\varphi'(z)} + \overline{\psi(z)} + \frac{E\alpha\sigma}{2\kappa} \overline{f(z)} F(z) = M^s \varepsilon_\theta^s e^{i\theta}. \quad (44)$$

Substituting (40)–(42) into (44), and noting that

$$e^{i\theta} = \frac{w\omega'(w)}{\rho|\omega'(w)|}, \quad e^{2i\theta} = \frac{w^2\omega'(w)}{\rho^2\overline{\omega'(w)}}, \quad (45)$$

we have

$$\begin{aligned}
& \varphi(w) + \frac{\omega(w)}{\omega'(w)} \overline{\varphi'(w)} + \overline{\psi(w)} + \frac{E\alpha\sigma}{2\kappa} \overline{f(w)} F(w) \\
&= M^s \left\{ \frac{1-\mu}{E} \left(\frac{w}{|\omega'(w)|} \varphi'(w) + \frac{w\omega'(w)}{|\omega'(w)|\overline{\omega'(w)}} \overline{\omega'(w)} + \frac{E\alpha\sigma}{2\kappa} \frac{w\omega'(w)}{|\omega'(w)|} |f(w)|^2 \right) \right. \\
&\quad + 4G \left(\frac{w^3}{\omega'(w)} \varphi''(w) - \frac{w^3\omega''(w)}{\omega'(w)} \varphi'(w) + \frac{w^3\omega'(w)}{|\omega'(w)|\overline{\omega'(w)}} \overline{\psi'(w)} \right. \\
&\quad \left. + \frac{\omega(w)}{w|\omega'(w)|\overline{\omega'(w)}} \overline{\varphi''(w)} - \frac{\omega(w)\overline{\omega''(w)}}{w|\omega'(w)|\overline{\omega'(w)}} \overline{\varphi'(w)} + \frac{1}{w|\omega'(w)|} \overline{\psi'(w)} \right) \\
&\quad - \frac{E\alpha\sigma}{8G\kappa} \frac{w\omega'(w)}{|\omega'(w)|\overline{\omega'(w)}} (A_1 w^2 - \bar{A}_1) \int \left[\left(\frac{A_1}{w} + \frac{\bar{A}_1}{w^3} \right) \bar{w} \left(\frac{1}{w} \right) \right] dw \\
&\quad + \frac{8\alpha\sigma}{8G\kappa} \frac{(\bar{A}_1 - A_1 w^2)}{w|\omega'(w)|} \int \left[\left(A_1 w + \frac{\bar{A}_1}{w} \right) \omega'(w) \right] dw \\
&\quad \left. + 2\alpha \frac{w\omega'(w)}{|\omega'(w)|} \operatorname{Re} \left[B_2 w^2 + B_1 w + \frac{\bar{B}_1}{w} + \frac{\bar{B}_2}{w^2} \right] \right\}. \quad (46)
\end{aligned}$$

We introduce Fourier series expansions for the w -related terms as

$$\begin{cases} \frac{1}{\omega'(w)} = \sum_{j=-n'}^{n'} \left(\frac{1}{2\pi} \int_0^{2\pi} \frac{\zeta^{-j}}{\omega'(\zeta)} d\theta \right) w^j, \\ \frac{1}{|\omega'(w)|} = \sum_{j=-n'}^{n'} \left(\frac{1}{2\pi} \int_0^{2\pi} \frac{\zeta^{-j}}{|\omega'(\zeta)|} d\theta \right) w^j, \\ \frac{1}{|\omega'(w)|\overline{\omega'(w)}} = \sum_{j=-n'}^{n'} \left(\frac{1}{2\pi} \int_0^{2\pi} \frac{\zeta^{-j}}{|\omega'(\zeta)|\overline{\omega'(\zeta)}} d\theta \right) w^j, \end{cases} \quad (47)$$

where $\zeta = e^{i\theta}$, and n' is selected to cover the highest power of w in (46). Since the multivalued terms in (46) will cancel each other on L , the stress boundary condition is successfully written in terms of Fourier series using (47). Equating coefficients of w^j ($j = -n, \dots, -1, 1, \dots, n$) in (46), we arrive at a system of equations with respect to C_{-j} and D_{-j} ($j = 1, \dots, n$). Solving this system numerically, the complex functions $\varphi(z)$ and $\psi(z)$ are determined completely.

4. Numerical analyses and discussion

Numerical analysis is undertaken to illustrate the distribution of thermal stress around the nanohole using the material parameters listed in Table 1. For illustrative purposes, we consider the stresses around an elliptic hole, an approximately triangular hole (which we refer to as a ‘triangular hole’) and an approximately square hole (similarly referred to as a ‘square hole’) and prescribe remote electric current and energy flux in the y -direction. The conformal mapping functions corresponding to the three shapes are given by [Savin 1961]

$$\begin{cases} \omega(w) = R(w + 1/3w), & \text{elliptic hole,} \\ \omega(w) = R(w + 1/3iw^2), & \text{triangular hole,} \\ \omega(w) = R(w - 1/8w^3), & \text{square hole,} \end{cases} \quad (48)$$

sample	σ (S/m)	S (μ V/K)	κ (W/mK)	E (GPa)	α (/K)	μ	M^s (N/m)
PbTe	10^4	300	1.5	58	$2 \cdot 10^{-5}$	0.29	10

Table 1. Material parameters of samples [Pei and Liu 2012; Ni et al. 2010].

with the area of these holes given by

$$s = \pi R^2(1 - jm_j^2), \quad (49)$$

where j corresponds to w^{-j} appearing in the conformal mapping function, and m_j is the coefficient of w^{-j} .

Comparing the state of stress around a macrohole, we can see that the surface elasticity mainly induces normal and shear stresses on the boundary of a nanohole. Consequently, we focus our investigation on the effect of electric current on the normal and shear stresses induced by surface elasticity for holes of different shapes as described in figures 2–4. In order to compare the stress fields for different shapes of hole, we set the area of each hole to be uniform at $s = 3 \text{ nm}^2$ and subject the thermoelectric material to a remote energy flux given by $U_y^\infty = 10^{-6} \text{ W/nm}^2$. For the case of an elliptic hole, the maximum positive and negative normal stresses induced by surface elasticity appear at the locations $\theta = 0.1\pi$ and -0.1π , respectively, while the maximum shear stress appears at $\theta = 0$ (see Figure 2). The remote electric current has considerable influence on the normal stress, but no influence on the shear stress. In addition, our results also show that the remote electric current has the capability of suppressing the absolute value of the negative normal stress and enhancing the positive normal stress around an elliptic hole.

For the same conditions used in Figure 2, the surface elasticity generates more than 10 times the normal and shear stresses on the boundary of a triangular hole than the on the boundary of an elliptic hole (see Figure 3). With the increase of remote electric current density, the maximum normal and shear stresses transfer from the lower boundary ($-\pi/2 < \theta < 0$) to the upper boundary ($0 < \theta \leq \pi/2$) of a triangular hole and the maximum normal stress is enhanced by a factor of 3 when the remote electric current density changes from 0 to $2 \cdot 10^{-6} \text{ A/nm}^2$. In contrast to the elliptic hole, the maximum shear stress does not occur at the tip (the point of maximum curvature) of a triangular hole, as we can see from Figure 3 (right). It is worth pointing out from Figure 3 (right) that an appropriate electric current density can suppress the maximum shear stress on the boundary of the triangular hole. The remote electric

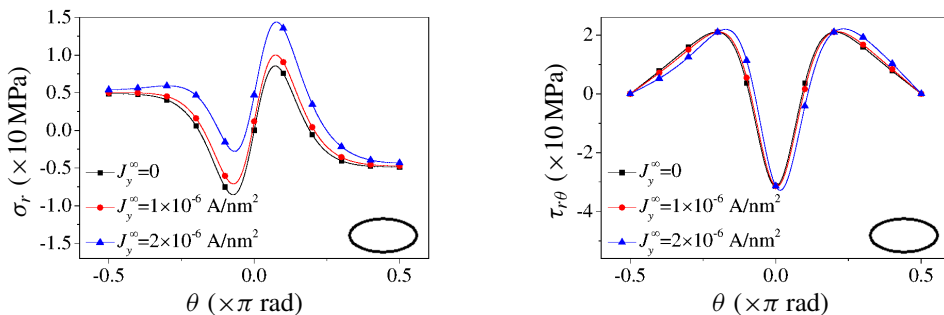


Figure 2. Normal stress (left) and shear stress (right) on the boundary of an elliptic hole.

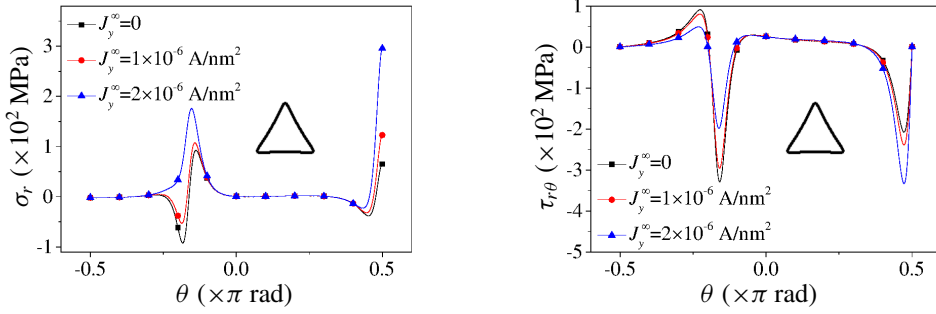


Figure 3. Normal stress (left) and shear stress (right) on the boundary of a triangular hole.

current suppresses maximum shear stress when $J_y^\infty = 10^{-6}$ A/nm² but enhances maximum shear stress for the case when $J_y^\infty = 2 \cdot 10^{-6}$ A/nm².

The normal and shear stresses around a square hole under various values of electric current are shown in Figure 4. Comparing with figures 2 and 3 we see that the maximum normal and shear stresses induced by surface elasticity around a square hole are higher than the maximum stress around an elliptic hole although much lower than the case of a triangular hole which corresponds with the order of their maximum curvatures. Figure 4 (left) shows that the electric current greatly enhances the normal stress on the lower boundary yet suppresses normal stress on the upper boundary of a square hole. In contrast, the electric current decreases and increases shear stress on the lower and upper boundary of a square hole, respectively, as shown in Figure 4 (right).

In Figure 5, $\sigma_r^{(1)}$ and $\tau_{r\theta}^{(1)}$ are the maximum normal and shear stresses on L when $R = 1$ nm. In figures 5 and 6, we further investigate the effect of surface elasticity on thermal stress with hole size. The value of the prescribed energy flux is adjusted to control the maximum temperature difference on the boundary of the hole at 1 K and the applied electric current density is adjusted to the optimal value around the hole. As is clear from Figure 5 (left), all of the maximum normal stresses decrease sharply with the increase in R , and tend to zero when $R = 20$ nm. The size of the hole has a stronger influence on the maximum normal stress around a square hole than on that around a triangular hole. Figure 5 (right) shows that the maximum shear stresses on the boundaries of elliptic and square holes decrease with the increase of R , which is the same as for normal stress. However, in the case of a triangular hole, the maximum shear stress increases in the initial phase of the increase in size of the hole: this is because the maximum shear

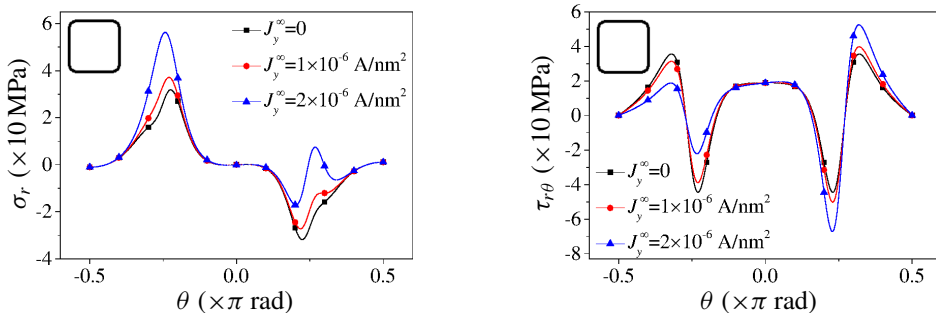


Figure 4. Normal stress (left) and shear stress (right) on the boundary of a square hole.

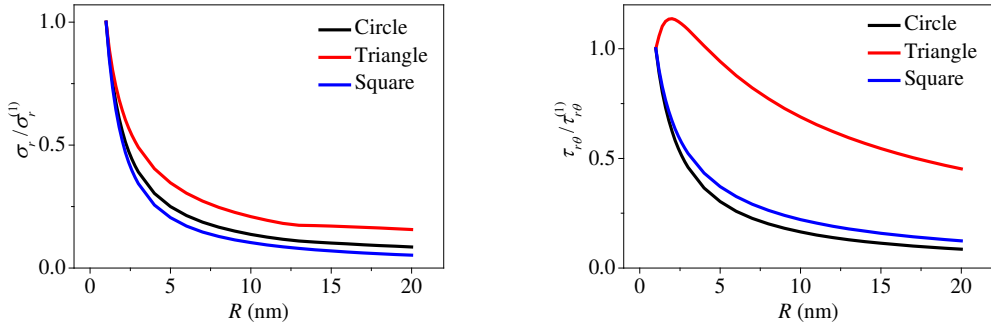


Figure 5. Maximum normal stress (left) and shear stress (right) versus R for different shaped holes.

stress occurs at the point of lower curvature on the boundary of triangular hole. With further increase of R , the effect of surface elasticity fades away, thus leading to a decrease of shear stresses for all shapes of hole.

In Figure 6, $\sigma_\theta^{(0)}$ and $\sigma_v^{(0)}$ are the maximum hoop and von Mises stresses on L when $M^s = 0$. We see from Figure 6 that surface elasticity has the ability to suppress maximum hoop stress induced by heat flux around nanoholes. This effect is more obvious around a triangular hole where the maximum hoop stress can be decreased by more than 50% as a result of surface elasticity. Even for the case of a square hole, the contribution of surface elasticity can decrease the maximum hoop stress by about 20%. Since the von Mises fracture criterion is often used in semiconductors, we also illustrate the effect of hole size on the von Mises stress σ_v using the expression [Yang 1980]:

$$\sigma_v = \sqrt{\sigma_x^2 - \sigma_x \sigma_y + \sigma_y^2 + 3\tau_{xy}^2}. \quad (50)$$

From Figure 6 (right) we see that surface elasticity can effectively suppress the maximum von Mises stress for all shapes of nanoholes. However, a particular size of nanohole is required for maximum effectiveness. For example, when $R = 2.5$ nm, the maximum von Mises stress generated by the heat flux is reduced by no more than 65% around a triangular hole.

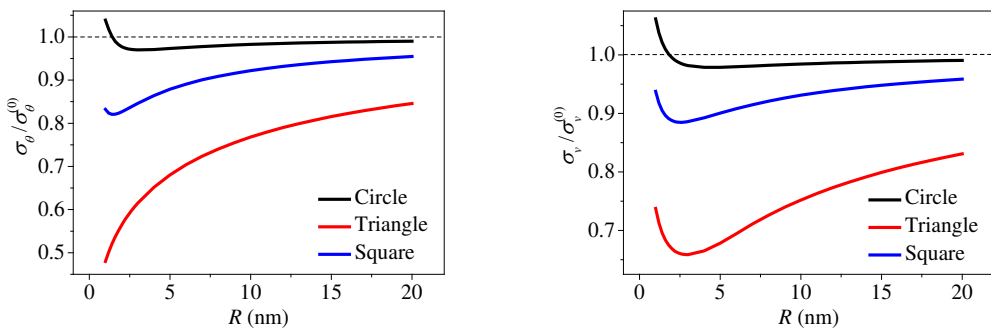


Figure 6. Maximum hoop stress (left) and von Mises stress (right) versus R for different shaped holes.

5. Conclusions

In this paper, we analyze the effect of surface elasticity on the thermal stress distribution around an arbitrarily shaped nanohole in a thermoelectric material. The electric, thermal and elastic fields in the matrix surrounding the nanohole are calculated based on complex variable methods. For a given area of nanohole, the surface elasticity generates higher normal and shear stresses around a triangular hole, but lower stresses around an elliptic hole which corresponds to the sequence of maximum curvature of the different hole shapes. The applied remote electric current can enhance or suppress the effect of surface elasticity on the thermal stress, depending on the shape and position of the boundary of the nanoholes. Detailed results show that surface elasticity has the ability of suppressing maximum hoop stress induced by heat flux around a nanohole, thus leading to significant reduction in von Mises stress. Accompanied by the appropriately chosen size of hole, surface elasticity can suppress the maximum von Mises stress around a triangular hole only by around 65%.

Acknowledgements

K. Song appreciates the support of the China Scholarship Council. H.-P. Song and Gao acknowledge the support of the National Natural Science Foundation of China (Grant no. 11872203 and 11202099), the Priority Academic Program Development of Jiangsu Higher Education Institutions (PAPD). Schiavone thanks the Natural Sciences and Engineering Research Council of Canada for their support through a Discovery Grant (Grant no. RGPIN 155112).

References

- [Attia 2017] M. A. Attia, “On the mechanics of functionally graded nanobeams with the account of surface elasticity”, *Int. J. Eng. Sci.* **115** (2017), 73–101.
- [Callen 1960] H. B. Callen, *Thermodynamics: an introduction to the physical theories of equilibrium thermostatics and irreversible thermodynamics*, John Wiley & Sons, New York, 1960.
- [Dai et al. 2016] M. Dai, P. Schiavone, and C.-F. Gao, “Uniqueness of neutral elastic circular nano-inhomogeneities in antiplane shear and plane deformations”, *J. Appl. Mech. (ASME)* **83**:10 (2016), 101001.
- [Dai et al. 2017] M. Dai, C.-F. Gao, and P. Schiavone, “Closed-form solution for a circular nano-inhomogeneity with interface effects in an elastic plane under uniform remote heat flux”, *IMA J. Appl. Math.* **82**:2 (2017), 384–395.
- [Gurtin and Murdoch 1975] M. E. Gurtin and A. I. Murdoch, “A continuum theory of elastic material surfaces”, *Arch. Ration. Mech. Anal.* **57**:4 (1975), 291–323.
- [Gurtin et al. 1998] M. E. Gurtin, J. Weissmüller, and F. Larché, “A general theory of curved deformable interfaces in solids at equilibrium”, *Philos. Mag. A* **78**:5 (1998), 1093–1109.
- [He and Tritt 2017] J. He and T. M. Tritt, “Advances in thermoelectric materials research: looking back and moving forward”, *Science* **357**:6358 (2017), eaak9997.
- [Kim et al. 2006] W. Kim, J. Zide, A. Gossard, D. Klenov, S. Stemmer, A. Shakouri, and A. Majumdar, “Thermal conductivity reduction and thermoelectric figure of merit increase by embedding nanoparticles in crystalline semiconductors”, *Phys. Rev. Lett.* **96**:4 (2006), 045901.
- [Kim et al. 2016] H. S. Kim, T. Wang, W. Liu, and Z. Ren, “Engineering thermal conductivity for balancing between reliability and performance of bulk thermoelectric generators”, *Adv. Funct. Mater.* **26**:21 (2016), 3678–3686.
- [Muskhelishvili 1975] N. I. Muskhelishvili, *Some basic problems of the mathematical theory of elasticity*, Noordhoff, Leyden, 1975.

- [Ni et al. 2010] J. E. Ni, E. D. Case, K. N. Khabir, R. C. Stewart, C.-I. Wu, T. P. Hogan, E. J. Timm, S. N. Girard, and M. G. Kanatzidis, “Room temperature Young’s modulus, shear modulus, Poisson’s ratio and hardness of PbTe–PbS thermoelectric materials”, *Mater. Sci. Eng. B* **170**:1–3 (2010), 58–66.
- [Özdemir et al. 2015] A. E. Özdemir, Y. Köysal, E. Özbaş, and T. Atalay, “The experimental design of solar heating thermoelectric generator with wind cooling chimney”, *Energy Convers. Manag.* **98** (2015), 127–133.
- [Pang et al. 2018] S.-J. Pang, Y.-T. Zhou, and F.-J. Li, “Analytic solutions of thermoelectric materials containing a circular hole with a straight crack”, *Int. J. Mech. Sci.* **144** (2018), 731–738.
- [Parkus 1968] H. Parkus, *Thermoelasticity*, Blaisdell Publishing Company, Waltham, Massachusetts, 1968.
- [Pei and Liu 2012] Y.-L. Pei and Y. Liu, “Electrical and thermal transport properties of Pb-based chalcogenides: PbTe, PbSe, and PbS”, *J. Alloy. Compd.* **514** (2012), 40–44.
- [Savin 1961] G. N. Savin, *Stress concentration around holes*, Pergamon Press, New York, 1961.
- [Song et al. 2015] H.-P. Song, C.-F. Gao, and J. Li, “Two-dimensional problem of a crack in thermoelectric materials”, *J. Therm. Stresses* **38**:3 (2015), 325–337.
- [Song et al. 2018] K. Song, H. P. Song, and C. F. Gao, “Improving compatibility between thermoelectric components through current refraction”, *Chin. Phys. B* **27**:7 (2018), 077304.
- [Song et al. 2019a] H. Song, K. Song, and C. Gao, “Temperature and thermal stress around an elliptic functional defect in a thermoelectric material”, *Mech. Mater.* **130** (2019), 58–64.
- [Song et al. 2019b] K. Song, H. P. Song, M. Li, P. Schiavone, and C. F. Gao, “Effective properties of a thermoelectric composite containing an elliptic inhomogeneity”, *Int. J. Heat Mass Transf.* **135** (2019), 1319–1326.
- [Song et al. 2019c] K. Song, H. P. Song, P. Schiavone, and C. F. Gao, “Electric current induced thermal stress around a bi-material interface crack”, *Eng. Fract. Mech.* **208** (2019), 1–12.
- [Wang and Wang 2017] P. Wang and B. L. Wang, “Thermoelectric fields and associated thermal stresses for an inclined elliptic hole in thermoelectric materials”, *Int. J. Eng. Sci.* **119** (2017), 93–108.
- [Xu et al. 2017] B. Xu, M. T. Agne, T. Feng, T. C. Chasapis, X. Ruan, Y. Zhou, H. Zheng, J.-H. Bahk, M. G. Kanatzidis, G. J. Snyder, and Y. Wu, “Nanocomposites from solution-synthesized PbTe–BiSbTe nanoheterostructure with unity figure of merit at low-medium temperatures (500–600 K)”, *Adv. Mater.* **29**:10 (2017), 1605140.
- [Yang 1980] W. H. Yang, “A generalized von Mises criterion for yield and fracture”, *J. Appl. Mech. (ASME)* **47**:2 (1980), 297–300.
- [Yang et al. 2015] L. Yang, Z. G. Chen, M. Hong, G. Han, and J. Zou, “Enhanced thermoelectric performance of nanostructured Bi₂Te₃ through significant phonon scattering”, *ACS Appl. Mater. Interfaces* **7**:42 (2015), 23694–23699.
- [Yu et al. 2015] S. Yu, Q. Du, H. Diao, G. Shu, and K. Jiao, “Start-up modes of thermoelectric generator based on vehicle exhaust waste heat recovery”, *Appl. Energy* **138** (2015), 276–290.
- [Zhang and Wang 2016] A. B. Zhang and B. L. Wang, “Explicit solutions of an elliptic hole or a crack problem in thermoelectric materials”, *Eng. Fract. Mech.* **151** (2016), 11–21.

Received 5 Aug 2019. Accepted 9 Sep 2019.

KUN SONG: ksong3@ualberta.ca

State Key Laboratory of Mechanics and Control of Mechanical Structures, Nanjing University of Aeronautics and Astronautics, Nanjing, 210016, China

HAO-PENG SONG: hpsong@nuaa.edu.cn

Department of Software Engineering, Nanjing University of Aeronautics and Astronautics, Nanjing, 210016, China

PETER SCHIAVONE: pschiavo@ualberta.ca

Department of Mechanical Engineering, University of Alberta, 10-203 Donadeo Innovation Center for Engineering, 9211-116 Street NW, Edmonton AB T6G 1H9, Canada

CUN-FA GAO: cfgao@nuaa.edu.cn

State Key Laboratory of Mechanics and Control of Mechanical Structures, Nanjing University of Aeronautics and Astronautics, Nanjing, 210016, China

JOURNAL OF MECHANICS OF MATERIALS AND STRUCTURES

msp.org/jomms

Founded by Charles R. Steele and Marie-Louise Steele

EDITORIAL BOARD

ADAIR R. AGUIAR	University of São Paulo at São Carlos, Brazil
KATIA BERTOLDI	Harvard University, USA
DAVIDE BIGONI	University of Trento, Italy
MAENGHYO CHO	Seoul National University, Korea
HUILING DUAN	Beijing University
YIBIN FU	Keele University, UK
IWONA JASIUK	University of Illinois at Urbana-Champaign, USA
DENNIS KOCHMANN	ETH Zurich
MITSUTOSHI KURODA	Yamagata University, Japan
CHEE W. LIM	City University of Hong Kong
ZISHUN LIU	Xi'an Jiaotong University, China
THOMAS J. PENCE	Michigan State University, USA
GIANNI ROYER-CARFAGNI	Università degli studi di Parma, Italy
DAVID STEIGMANN	University of California at Berkeley, USA
PAUL STEINMANN	Friedrich-Alexander-Universität Erlangen-Nürnberg, Germany
KENJIRO TERADA	Tohoku University, Japan

ADVISORY BOARD

J. P. CARTER	University of Sydney, Australia
D. H. HODGES	Georgia Institute of Technology, USA
J. HUTCHINSON	Harvard University, USA
D. PAMPLONA	Universidade Católica do Rio de Janeiro, Brazil
M. B. RUBIN	Technion, Haifa, Israel

PRODUCTION production@msp.org

SILVIO LEVY Scientific Editor


Cover photo: Mando Gomez, www.mandolux.com

See msp.org/jomms for submission guidelines.

JoMMS (ISSN 1559-3959) at Mathematical Sciences Publishers, 798 Evans Hall #6840, c/o University of California, Berkeley, CA 94720-3840, is published in 10 issues a year. The subscription price for 2019 is US \$635/year for the electronic version, and \$795/year (+\$60, if shipping outside the US) for print and electronic. Subscriptions, requests for back issues, and changes of address should be sent to MSP.

JoMMS peer-review and production is managed by EditFlow® from Mathematical Sciences Publishers.

PUBLISHED BY

 **mathematical sciences publishers**
nonprofit scientific publishing

<http://msp.org/>

© 2019 Mathematical Sciences Publishers

Extended higher-order sandwich panel theory for plates with arbitrary aspect ratios	FAISAL SIDDIQUI and GEORGE A. KARDOMATEAS	449
Applications of extended higher order sandwich panel theory for plates with arbitrary aspect ratios	FAISAL SIDDIQUI and GEORGE A. KARDOMATEAS	461
Instabilities in the free inflation of a nonlinear hyperelastic toroidal membrane	SAIRAM PAMULAPARTHI VENKATA and PRASHANT SAXENA	473
Plane strain polar elasticity of fibre-reinforced functionally graded materials and structures	KONSTANTINOS P. SOLDATOS, METIN AYDOGDU and UFUK GUL	497
Integrated modelling of tool wear and microstructural evolution internal relations in friction stir welding with worn pin profiles	ZHAO ZHANG and ZHIJUN TAN	537
Local gradient theory for thermoelastic dielectrics: accounting for mass and electric charge transfer due to microstructure changes	OLHA HRYTSYNA and VASYL KONDRAT	549
The effect of boundary conditions on the lowest vibration modes of strongly inhomogeneous beams	ONUR ŞAHİN	569
Thermal stress around an arbitrary shaped nanohole with surface elasticity in a thermoelectric material	KUN SONG, HAO-PENG SONG, PETER SCHIAVONE and CUN-FA GAO	587